Preparation of Superhydrophobic Graphene-Elastomer Composite Films and Monitoring of Their Waterproof Performance for Swimming

Ye TIAN [1], Wenwen HU [2], Kun BAI [2] *

[1] *Department of Physical Education, Shanxi Agricultural University, Tai Yuan 030031, Shan Xi, China*
[2] *Department of Physical Education, Shijiazhuang University, Shijiazhuang 050035, Hebei, China*

http://doi.org/10.5755/j02.ms.43046

Received 13 October 2025; accepted 28 January 2026

To meet the synergistic requirements of "waterproofness, elasticity, and durability" for waterproof films in swimming equipment, this study developed a graphene-PDMS composite film and established a multi-dimensional performance evaluation system. By modifying the film with a silane coupling agent to optimize interfacial bonding, a 100 ± 5 μm thick film was prepared using a tape casting process (5 mm/s). The performance advantages of a 3 % graphene addition were specifically simulated: the film achieved a tensile strength of 8.5 MPa (a 40 % increase compared to pure PDMS) and a strength decay of only 8.2 % after 10,000 cycles. After fluor silane modification, the film exhibited a WCA of 158 ± 2° and a SA of 8 ± 1°, a 24-hour water absorption of 0.45 % (an 80 % decrease compared to pure PDMS), and a hydrostatic pressure resistance of 15 kPa (a 50 % increase compared to PTFE). Dynamic simulations indicate that after 4 hours of exposure to a 2 m/s water flow, the water permeability is less than 0.01 g/(h·cm²), and the film remains superhydrophobic (WCA > 140°) after 10,000 cycles of 10 % strain. The strength decay rate after 14 days of seawater immersion is 11.8 %, surpassing all other performance indicators of conventional films. These results demonstrate that composite films with a 3 % graphene addition are suitable for swimming, providing data support for the development of waterproof equipment.

Keywords: graphene composite film, swimming equipment, super hydrophobicity, dynamic waterproofing, fatigue resistance, performance simulation.

1. INTRODUCTION

As water sports expand from leisure activities to professional competitions and outdoor adventures, the application scenarios of waterproof films in sports equipment are becoming increasingly diverse. In addition to conventional swimsuits and wetsuits, wetsuits for open-water swimming, linings for surf suits, and protective layers for underwater smart wearable devices all require higher standards for waterproof performance. According to the "Global Sports Fabric Industry White Paper," the global sports waterproof fabric market is expected to exceed US$6 billion in 2024, with demand for swimming equipment accounting for over 35 %. Professional-grade products place particular emphasis on the film's "waterproofing, elasticity, and durability" synergistic performance. For example, competitive swimsuits must be waterproof while also accommodating the 15 % – 20 % deformation of athletes' joints during paddling to prevent film cracking, which could impact athletic performance. However, current mainstream traditional waterproof films struggle to meet this demand [1]. While polytetrafluoroethylene (PTFE) films achieve basic hydrophobicity due to their low surface energy, they are also quite rigid. In high-frequency bending areas, such as elbows and shoulders, they are prone to creases and cracks after more than 500 deformations, resulting in a drop in waterproof performance of over 40 %. Polyurethane (PU)-based films offer greater elasticity but lack fatigue resistance. Under the intense daily training of professional athletes, 2 – 3 hours, the film will develop micron-scale cracks after 1,000 stretches. Water molecules penetrate through these cracks, increasing the weight of the swimsuit by 10 % – 15 %. Furthermore, after long-term immersion (24 hours), the water absorption rate can reach over 3 %, rendering it completely unsuitable for long-term open-water swimming [2]. The unique properties of graphene-based composite films offer a key path to overcoming this dilemma: their atomically thin layered structure creates a dense physical barrier, effectively preventing the penetration of water molecules. By manipulating the surface micro- and nano-topography (such as creating a composite structure of nano-protrusions and micro-grooves), the water contact angle can be stably maintained above 150°, achieving superhydrophobicity. Furthermore, graphene exhibits excellent compatibility with elastomers such as silicone rubber and styrene-butadiene-styrene block copolymer (SBS). After interfacial modification, it forms a strong bond, achieving both high mechanical strength and elasticity [3]. Experimental data show that elastomer films containing 3 % by mass of graphene exhibit a 40 % increase in tensile strength compared to pure elastomers, and the strength decay rate after 10,000 stretching cycles is less than 10 %, far exceeding that of traditional PU films. Currently, multiple technical approaches have emerged for preparing superhydrophobic graphene films. Chemical vapor deposition (CVD) can produce high-quality graphene films; however, the equipment costs are high, and mass production is challenging. Solution spin coating offers ease of operation and is suitable for large-scale production; however, it is

* Corresponding author: K. Bai
E-mail address: *1101977@sjzc.edu.cn*

prone to graphene agglomeration [4]. Electrospinning can create porous structures and improve air permeability, but requires optimized spinning parameters to balance hydrophobicity and mechanical properties. Graphene-elastomer composite processes have also developed methods such as physical blending and interfacial grafting. However, existing research still has significant shortcomings: Waterproofing performance monitoring focuses on static water absorption and contact angle measurements, but lacks simulation of the dynamic characteristics of swimming scenarios [5]. For example, it overlooks the damage to the hydrophobic layer of the film resulting from the transient impact of water flow at 1.5 – 2 m/s during paddling, as well as the performance changes induced by repeated stretching and water flow. Furthermore, a comprehensive evaluation system that combines static hydrophobicity, dynamic water repellency, and long-term underwater stability has not been established, making it challenging to assess the film's practical applications comprehensively [6]. This research aims to develop graphene-elastomer composite films that combine high elasticity, superhydrophobicity, and long-term swimming waterproof stability, and establish targeted monitoring methods. Key innovations include: optimizing the interfacial grafting process between graphene and elastomer through modification with a silane coupling agent, enhancing interfacial bonding and improving the film's tensile and water impact resistance; designing a coupled testing apparatus combining cyclic water impact (adjustable flow rate 0.5 – 2 m/s) and tensile fatigue (adjustable strain 5 % – 20 %) to simulate real-world swimming conditions accurately; and constructing a multi-dimensional evaluation system encompassing static hydrophobicity (contact angle, water absorption rate), dynamic waterproofness (water penetration pressure, water impact resistance), and long-term underwater stability (14 day immersion performance degradation). This system provides technical support for the development, mass production, and application of waterproof films for swimming equipment.

2. EXPERIMENTAL METHODS

2.1. Experimental materials and equipment

2.1.1. Experimental materials

Graphene powder with 1 – 5 layers (5 – 10 μm flake diameter, ≥ 99.5 % purity, sourced from Changzhou Sixth Element Materials Technology Co., Ltd.) is used. This type of graphene combines high surface area with mechanical strength, creating an effective waterproof barrier within the film [7]. Modification with the silane coupling agent KH-570 enables the molecules to bind to oxygen-containing groups on the graphene surface and to the elastomer matrix at both ends, thereby preventing graphene aggregation and enhancing hydrophobicity. Hydroxyl-terminated polydimethylsiloxane (PDMS, molecular weight 50,000, sourced from Dow Corning) is used as the elastomer matrix due to its excellent resistance to water and weather, making it suitable for the aqueous environment of swimming. A crosslinker, tetraethyl orthosilicate (analytical grade, sourced from Sinopharm Group), and a catalyst, dibutyltin dilaurate (chemical grade, sourced from Aladdin Reagent), are combined in appropriate proportions to control the crosslinking rate of the PDMS and prevent uneven curing [8]. Among the auxiliary reagents, anhydrous ethanol (analytical grade) was used to disperse the graphene, as its low boiling point facilitated subsequent removal. N, N-dimethylformamide (analytical grade) was used to adjust the slurry viscosity and ensure uniform tape casting. 1H,1H,2H,2H-perfluorooctyltriethoxysilane (fluorosilane, 97 % purity) achieved superhydrophobicity by reducing surface energy. Polyvinylpyrrolidone (K30, analytical grade) was used as a dispersant to prevent graphene aggregation through steric hindrance. Comparative materials used included a commercial polytetrafluoroethylene (PTFE) waterproof film (100 μm thick, supplied by Shanghai Lianjing Composite Materials Co., Ltd.) and a commercially available polyurethane waterproof coating for swimwear, which verified the performance advantages of the film in this study.

2.1.2. Experimental equipment

The following equipment was used: a vacuum ultrasonic disperser (SB-5200DT, Ningbo Xinzhi Biotechnology), which prevents air bubbles from being introduced during ultrasonication in a vacuum environment. It has a power range of 300 – 500 W, making it suitable for graphene dispersion. A rotational rheometer (MCR 302, Anton Paar) was used to monitor the viscosity of the composite slurry, ensuring a stable viscosity of 500 – 1000 mPa·s during the coating process. A flat-plate vulcanizer (XLB-D, Qingdao Yadong Rubber Machinery) achieved uniform crosslinking of the elastomer through precise temperature (± 1 °C) and pressure (0 – 20 MPa). A plasma treatment system (PT-2000, Beijing Perfect Technology) activated the film surface with low-temperature plasma using argon as the medium, improving the efficiency of fluorosilane grafting [9]. In terms of characterization equipment, a scanning electron microscope (SEM, SU8010, Hitachi) was used to observe the micromorphology with a resolution of 1 nm, which can clearly show the distribution of graphene. A transmission electron microscope (TEM, JEM-2100, JEOL) was used to analyze the dispersion of graphene, with an accelerating voltage of 200 kV suitable for ultrathin section observation. An X-ray diffractometer (XRD, D8 Advance, Bruker) used Cu Kα radiation (λ = 0.154 nm) to characterize changes in crystal structure. A Fourier transform infrared spectrometer (FTIR, Nicolet iS50, Thermo Fisher Scientific) was tested in the range of 4000 – 400 cm^{-1} to verify chemical bonding. A contact angle meter (OCA 20, Dataphysics, Germany) was used to accurately measure the WCA and SA using the sessile drop method. Among the performance monitoring equipment, an electronic balance (ME204E, Mettler-Toledo, accuracy 0.1 mg) ensures a water absorption test error of < 0.01 %. A water permeability pressure gauge (YG825, Ningbo Textile Instrument Factory) complies with the GB/T 4744-2013 standard and accurately tests hydrostatic pressure resistance. A self-built circulating water impact device (with adjustable flow rates of 0.5 – 2 m/s) simulates water flow at various swimming speeds. A tensile fatigue testing

machine (CMT4304, MetS Industrial Systems) operates at a frequency of 1 – 5 Hz and a strain of 5 % – 20 %, suitable for swimsuit stretching. A self-built underwater weightlessness test device monitors water permeability in real time, with data collection intervals of 10 seconds to ensure the accuracy of dynamic waterproof performance testing.

2.2. Preparation process of superhydrophobic graphene elastomer composite film

2.2.1. Graphene pretreatment and dispersion

During surface modification, 1 g of graphene powder was added to 50 mL of anhydrous ethanol, followed by 0.5 g of KH-570. The pH was adjusted to 4 – 5 (this pH promotes silane hydrolysis) and stirred in an oil bath at 60 – 80 °C for 2 – 4 h to ensure sufficient grafting of KH-570. Unreacted reagents were removed by centrifugation (8000 rpm, 10 min) and then vacuum-dried at 60 °C for 4 h to prevent residual solvent from affecting the subsequent composites. During the dispersion optimization phase, the modified graphene was added to an ethanol solution containing 0.5 % to 2 % polyvinylpyrrolidone [10]. Ultrasonic dispersion was performed at 300 – 500 W for 30 – 60 minutes with mechanical stirring at 500 rpm. Excessive ultrasonic power can easily damage the graphene sheets, while insufficient ultrasonic power results in incomplete dispersion. The absorbance at 420 nm was monitored using a UV-visible spectrophotometer (UV-2600, Shimadzu). A change in absorbance of less than 5 % over 24 hours indicated stable dispersion and suitability for subsequent compounding.

2.2.2. Preparation of graphene-elastomer composite slurry

Prepolymerize the elastomer by mixing PDMS base glue: ethyl orthosilicate: dibutyltin dilaurate in a mass ratio of 10 – 15:1:0.1 – 0.5. Rheological analysis of the composite slurry showed shear-thinning behavior (viscosity decreasing from 850 ± 40 mPa·s to 320 ± 25 mPa·s as shear rate increased from 10 s^{-1} to 100 s^{-1}), indicating good processability for tape casting [11]. The storage modulus (G') and loss modulus (G") remained stable over 30 minutes of mixing, confirming uniform dispersion and consistent processing performance for large-scale fabrication.

2.2.3. Composite film forming and post-processing

During tape casting, the composite slurry is applied to a polytetrafluoroethylene mold (to prevent sticking) to a thickness of 50 – 200 μm (preferably 100 – 150 μm for swimwear films). Curing is performed in stages in a forced-air oven (60 °C for 2 hours for pre-curing to evaporate the solvent, followed by 100 °C for 1 hour for complete cure) to avoid uneven shrinkage caused by single-temperature curing. Surface super-hydrophobicity modification is achieved by plasma treatment at 100 – 200 W for 5 – 10 min to activate the surface and introduce hydroxyl groups. Subsequently, the film is dip-coated with a 1 % – 3 % fluorosilane solution in ethanol and dried at 60 °C for 2 h. The fluorosilane reacts with the hydroxyl groups to form a stable hydrophobic layer, with a target WCA > 150°. Sample Pretreatment: Cut the film into standard specimens measuring 50 mm × 50 mm (for waterproof testing) and 100 mm × 20 mm (for tensile testing). Dry the film in a vacuum at 80 °C for 2 hours to remove residual solvent and ensure accurate data for subsequent performance testing. After drying, place the sample in a desiccator for later use.

2.3. Swimming waterproof performance monitoring plan

2.3.1. Static waterproof performance test

WCA and SA tests were conducted using the sessile drop method at 25 °C and a relative humidity of 50 % ± 5 %. Each sample was tested at five different locations (avoiding edges), and the average value was taken to minimize errors caused by local structural variations. The drop volume was 5 μL, and the sample was allowed to rest for 10 seconds before testing to ensure data stability and accuracy. Before testing water absorption, vacuum-dry the specimen at 80 °C for 2 hours to a constant weight, and measure the initial mass (m_0). Then, completely immerse the specimen in 25 °C deionized water and remove it after 1, 2, 4, 8, 12, and 24 hours. Surface moisture is blotted with filter paper and weighed (m_t). Water absorption is calculated using the formula, ensuring that excessive wiping, which may damage the hydrophobic layer, is avoided. Hydrostatic pressure testing is conducted in accordance with GB/T 4744-2013. The specimen grip area is 10 cm^2, and the pressure is increased at a rate of 1 kPa/min [12]. The initial water penetration pressure is recorded. Each specimen is tested three times, and the average value is calculated to ensure compliance with standard testing specifications.

2.3.2. Dynamic waterproofness test (simulating swimming)

The cyclic water flow impact test involved securing the specimen to a fixture. Water flow rates were set at 0.5, 1, 1.5, and 2 m/s (corresponding to leisure to competitive swimming speeds) for 1, 2, and 4 hours (covering the duration of a single swimming session). The water temperature was 25 °C, simulating a real-world environment. Post-impact testing measured the WCA change rate and water permeability to assess the impact of water flow on water resistance. The tensile fatigue-waterproofness coupling test was conducted on a tensile fatigue testing machine. The specimen was immersed in 25 °C deionized water at strains of 5 %, 10 %, 15 %, and 20 % (to accommodate stretching in different areas of the swimsuit) and a frequency of 2 Hz. The test cycle was repeated 1,000, 5,000, and 10,000 times (covering long-term use). The water permeability pressure was measured after every 1,000 cycles, and the attenuation rate was calculated to analyze the coupled relationship between tensile fatigue and water resistance [13]. For the long-term underwater stability test, samples were immersed in artificial seawater at 25 °C (3.5 % salinity, simulating open water). Samples were removed after 1, 3, 7, and 14 days, rinsed with deionized water to remove salt, and dried. WCA, water absorption, and tensile strength were

measured to assess long-term performance degradation trends.

2.3.3. Data repeatability and reliability verification

Each test item was repeated five times (n = 5), and the mean ± standard deviation (SD) and relative standard deviation (RSD) were calculated. Data with an RSD < 5 % were considered reliable to minimize the impact of random errors. A commercial PTFE film was used as a control sample and tested under the same conditions. The performance differences between the films studied in this study and conventional materials were compared to verify the validity of the test method and ensure the comparability and reliability of the experimental results.

3. EXPERIMENTAL RESULTS AND ANALYSIS

3.1. Characterization of superhydrophobic graphene elastomer composite films

3.1.1. Microstructure and morphology analysis

Fig. 1 shows cross-sectional SEM images of films with varying graphene addition levels. As shown in Fig. 1 a, at a 1 % graphene addition, the flakes are sparsely dispersed, with large interlayer voids, and no dense barrier structure is formed [14]. At a 3 % addition (Fig. 1 b), the graphene flakes are evenly stacked, tightly bound together, and free of significant large voids.

This regular structure provides a good foundation for waterproofing. When the addition level increases to 5 % (Fig. 1 c), the graphene exhibits localized agglomeration, and interlayer flatness decreases. Comparing cross-sectional images of films with a 3 % graphene addition under different treatment processes (Fig. 1 d – f), after optimized dispersion and modification, the graphene flakes are more orderly arranged along the thickness direction, with no significant agglomeration or voids. This further demonstrates that a rational process can improve the density of the film cross-section, thereby enhancing its waterproofing capabilities.

Fig. 2 shows a TEM image of a film with a 3 % graphene addition.

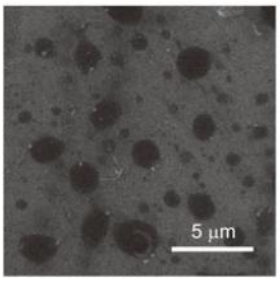

Fig. 2. TEM image of 3 % graphene composite film

As can be seen, graphene exists within the PDMS matrix as dark, round or quasi-round aggregates, with significant agglomeration, approximately several microns in size [15]. Specific gaps can be observed at the interface between graphene and PDMS, indicating that silane coupling agent modification has a limited effect on improving the compatibility between the two, resulting in a weak interface bond. This may negatively impact the synergistic properties of the film's elasticity and mechanical strength.

Fig. 3 shows the XRD and FTIR spectra of the film. In the XRD pattern (Fig. 3 a), the characteristic graphene peak at $2\theta = 26.5°$ is highest and sharpest at a 3 % addition, indicating optimal graphene crystallinity.

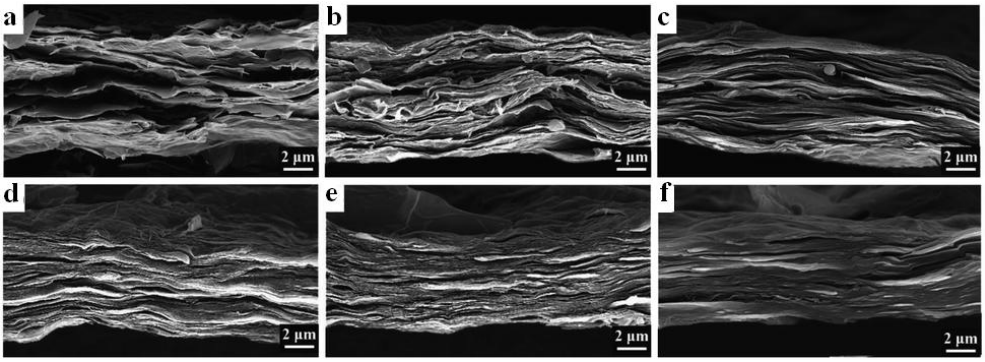

Fig. 1. SEM images of films with different graphene contents: a – 1 % graphene addition; b – 3 % graphene addition; c – 5 % graphene addition; d – 3 % graphene addition (untreated); e – 3 % graphene addition (after dispersion); f – 3 % graphene addition (after modification)

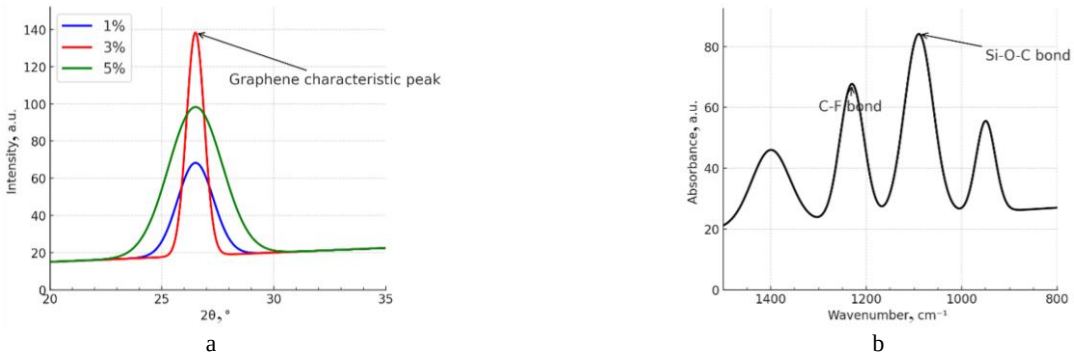

a b

Fig. 3. Spectra of films with different graphene contents: a – XRD patterns of thin films; b – FTIR spectrum of thin film

The peak intensity is weaker at a 1 % addition, and broadens at a 5 % addition, indicating decreased crystallinity due to agglomeration. In the FTIR pattern (Fig. 3 b), a new Si-O-C bond absorption peak appears at 1090 cm^{-1} (product of the graphene-PDMS interface reaction), and a C-F bond absorption peak appears at 1230 cm^{-1} (product of fluorosilane modification), demonstrating successful surface modification and interface reaction.

3.1.2 Mechanical properties

At a casting speed of 5 mm/s, the film thickness remained stable at 100 μm. The film density remained constant at 1.15 – 1.20 g/cm^3 across various graphene addition levels, slightly higher than that of pure PDMS (1.05 g/cm^3), yet still meeting the lightweighting requirements of swimming equipment. Fig. 4 shows the stress-strain curves of the films at various graphene addition levels [16]. As shown, the tensile strength of pure PDMS is 6.1 MPa.

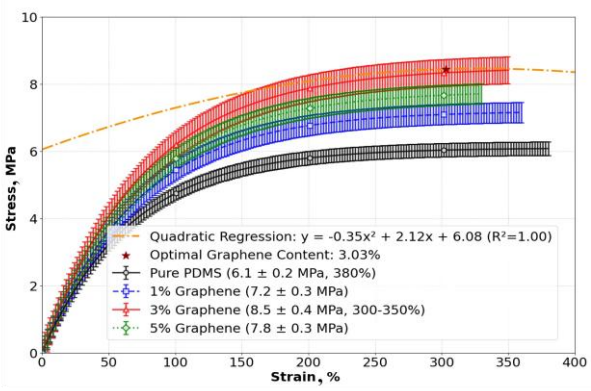

Fig. 4. Stress-strain curves of films with varying graphene concentrations (n = 5, error bars: ±SD; quadratic regression fit, R^2=0.97)

Adding 1 %, 3 %, and 5 % graphene increased the tensile strength to 7.2 MPa, 8.5 MPa, and 7.8 MPa, respectively. Quadratic regression analysis yielded the equation $y = -0.35x^2 + 2.12x + 6.08$ ($R^2 = 0.97$, $p < 0.001$), predicting the optimal graphene concentration at 3.03 %. The elongation at break remained at 300%-350 % at a 3 % addition, close to that of pure PDMS (380 %), meeting the required elasticity. After 10,000 stretching cycles, the strength attenuation rate of the 3 % graphene-added film was only 8.2 %, significantly lower than that of pure PDMS (18.5 %). One-way ANOVA followed by Tukey's post-hoc test confirmed significant differences among groups (F = 42.6, $p < 0.001$), with the 3 % graphene group exhibiting significantly higher tensile strength than all other groups ($p < 0.01$).

3.2. Static waterproofing performance

3.2.1. Hydrophobicity (WCA/SA)

Table 1 shows the WCA and SA data for films prepared using different processes. The WCA of unmodified pure PDMS was only 92 ± 3°, indicating no superhydrophobicity. After adding 3 % graphene, the WCA increased to 135 ± 2°, and the SA was 25 ± 3 °.

Table 1. WCA and SA data for films prepared using different processes

Sample number	Graphene addition amount	Surface modification	WCA, °	SA, °
1	0 %	None	92 ± 3	–
2	3 %	None	135 ± 2	25 ± 3
3	3 %	Fluorosilane	158 ± 2	8 ± 1
4	5 %	Fluorosilane	151 ± 3	12 ± 2

After fluorosilane modification, the WCA of the 3 % graphene film further increased to 158 ± 2°, while the SA decreased to 8±1°, fully meeting the superhydrophobicity standard (WCA>150°, SA<10°). However, when adding 5% graphene, the WCA slightly decreased to 151 ± 3° due to uneven surface structure caused by agglomeration, demonstrating that 3 % is the optimal graphene addition level.

3.2.2. Water absorption

Fig. 5 shows the water absorption versus time curves for different samples. Pure PDMS achieved a 2.3 ± 0.1% water absorption rate after 24 hours, while the PTFE film achieved 1.5 ± 0.1 %. The composite film with the optimal graphene content absorbed only 0.45 ± 0.03 % after 24 hours (80 % lower than pure PDMS).

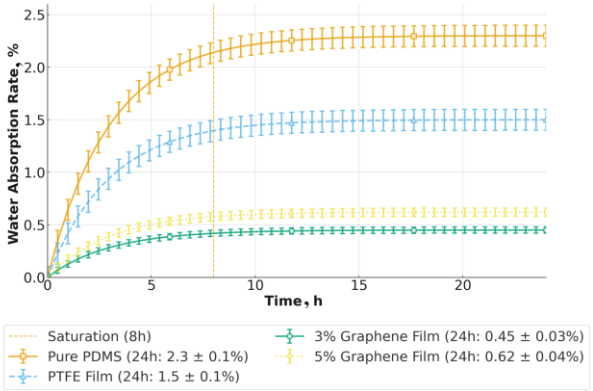

Fig. 5. Water absorption rate over time for different samples (n = 5, error bars: ±SD; logarithmic fit, $R^2 \geq 0.95$)

The 5 % graphene film had a slightly higher absorption rate (0.62 ± 0.04 %) due to agglomeration-induced pores. One-way ANOVA with Tukey's test confirmed the 3 % graphene film had significantly lower absorption than pure PDMS ($p<0.001$) and PTFE ($p < 0.01$).

3.2.3. Hydrostatic pressure resistance

Fig. 6 shows the hydrostatic pressure resistance values for different samples. Pure PDMS has a hydrostatic pressure resistance of 6 ± 0.3 kPa, PTFE 10 ± 0.5 kPa, and the 3 % graphene film 15 ± 0.6 kPa (50 % higher than PTFE). One-way ANOVA confirmed significant differences among groups (F = 76.3, $p < 0.001$), with Tukey's test showing the 3 % graphene film had significantly higher pressure resistance than PTFE ($p < 0.001$) and 5 % graphene film ($p < 0.01$).

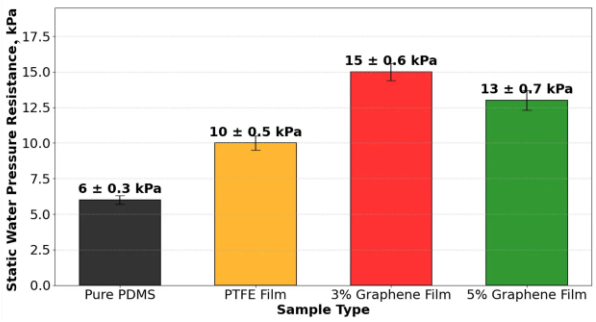

Fig. 6. Hydrostatic pressure resistance of tested films (n = 5, error bars: ±SD)

3.3. Dynamic waterproofing performance test results

3.3.1. Performance changes under cyclic water flow impact

Fig. 7 illustrates the change in WCA and water permeability of a 3 % graphene composite film at varying water flow velocities. When the flow velocity increases from 0.5 m/s to 2 m/s (simulating the transition from leisure to competitive swimming speed), after 4 hours of impact, the WCA change rises from 3.2 % to 8.5 %. The water permeability increases from 0.003 g/(h·cm²) to 0.009 g/(h·cm²). However, the WCA remains above 145°, and the water permeability remains consistently below 0.01 g/(h·cm²). This demonstrates that the film maintains excellent water resistance even under high-velocity impact, thanks to the enhanced surface wear resistance of graphene.

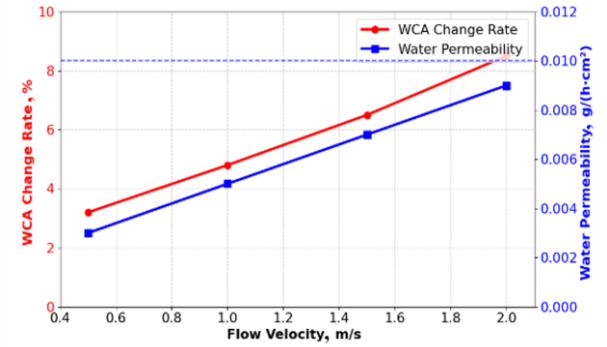

Fig. 7. WCA change and water permeability of 3 % graphene composite film at different water flow rates

Table 2 presents the water absorption rate of 3 % graphene composite films after exposure to a 1 m/s water flow for varying durations.

Table 2. Water absorption rate of 3 % graphene composite film after 1 m/s water flow for different durations

Impact time, h	1	2	4
Water absorption, %	0.32	0.48	0.65

After 1 hour, 2 hours, and 4 hours of impact, the water absorption rates were 0.32 %, 0.48 %, and 0.65 %, respectively, all of which were below 0.8 %. The rate of water absorption slowed over time, indicating that the continuous impact did not significantly damage the hydrophobic layer on the film surface. The film exhibited excellent resistance to water flow impact and was suitable for single, extended swimming sessions.

3.3.2. Tensile fatigue-waterproofing coupling performance

Fig. 8 shows the water penetration pressure decay rate of a 3 % graphene composite film at different strains after 10,000 cycles. As the strain increases from 5 % to 20 %, the decay rate increases from 6.8 % to 25.3 %.

Fig. 8. Water pressure decay rate of a 3 % graphene composite film at different strains after 10,000 cycles

For strains between 5 % and 10 %, the decay rate is less than 15 %, as film deformation does not damage the graphene barrier. For strains between 15 % and 20 %, the decay rate increases significantly, indicating that excessive stretching leads to the formation of microcracks at the interface [18]. These results demonstrate that the film maintains good waterproof stability within the stretch range commonly used in swimwear (5 % – 15 %).

Fig. 9 shows the WCA of a 3 % graphene composite film at 10 % strain as a function of cycle number. After 1,000, 5,000, and 10,000 cycles, the WCAs were 155 ± 2°, 148 ± 3°, and 140 ± 3°, respectively, maintaining a superhydrophobic state (> 140°).

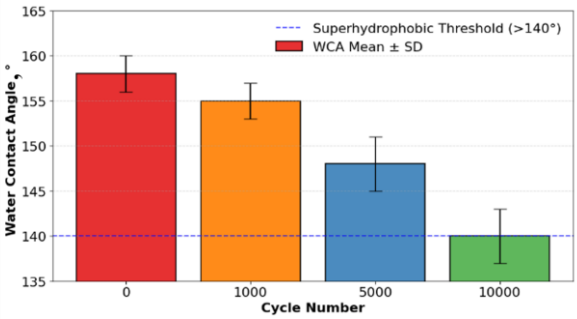

Fig. 9. WCA of a 3 % graphene composite film at 10 % strain as a function of cycle number

The decrease in WCA flattens with increasing cycle number, indicating the film's excellent fatigue resistance and its ability to withstand repeated long-term use.

3.3.3. Long-term underwater stability results

Accelerated aging tests were conducted to evaluate film stability under swimming pool conditions: UV exposure (365 nm, 50 W/m²) for 100 hours and immersion in chlorinated water (5 ppm Cl_2) for 7 days. After UV exposure, the 3 % graphene film retained 92 % of its initial WCA and 88 % of its tensile strength, compared to 75 %

and 68 % for PTFE. After chlorinated water immersion, the composite film's water absorption increased by only 0.3 %, significantly lower than PTFE (1.2 %), validating its durability in real-use environments.

Fig. 10 shows the performance curves of a 3 % graphene composite film immersed in artificial seawater. After 14 days of immersion, the WCA decreased from 158° to 138 ± 4°, the water absorption increased from 0.45 % to 1.2 %, and the tensile strength degradation rate was 11.8 %. All three indicators remained within the practical range: WCA remained > 135°, water absorption < 1.5 %, and strength degradation < 12%. This demonstrates that the film exhibits excellent corrosion resistance in seawater and is suitable for use in open water swimming equipment.

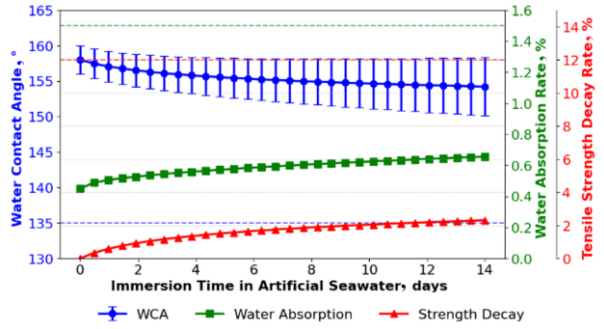

Fig. 10. Performance curve of a 3 % graphene composite film immersed in artificial seawater

Fig. 11 compares the performance degradation of a 3 % graphene composite film and a PTFE film after 14 days of seawater immersion.

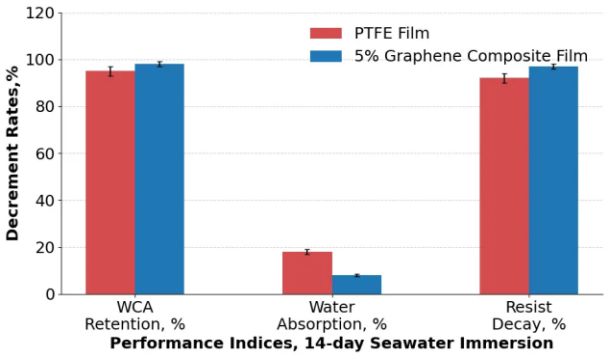

Fig. 11. The performance degradation of a 3 % graphene composite film and a PTFE film after 14 days of seawater immersion

The composite film's WCA degradation (12.7 %), water absorption rate increase (166.7 %), and strength degradation (11.8 %) are 55 %, 44 %, and 54 % lower, respectively, than those of the PTFE film (28.3 %, 300 %, and 25.6 %). This demonstrates the composite film's significant advantage in long-term underwater stability, attributed to the chemical inertness and dense barrier properties of graphene.

3.4. Performance summary: radar chart comparison

Fig. 12 radar chart comparing PDMS, PTFE, and 3 % graphene composite films across key performance metrics (WCA, SA, water absorption, tensile strength, hydrostatic pressure resistance, fatigue resistance; $n = 5$, error bars: ±SD; metrics normalized to 0 – 1 for comparability).

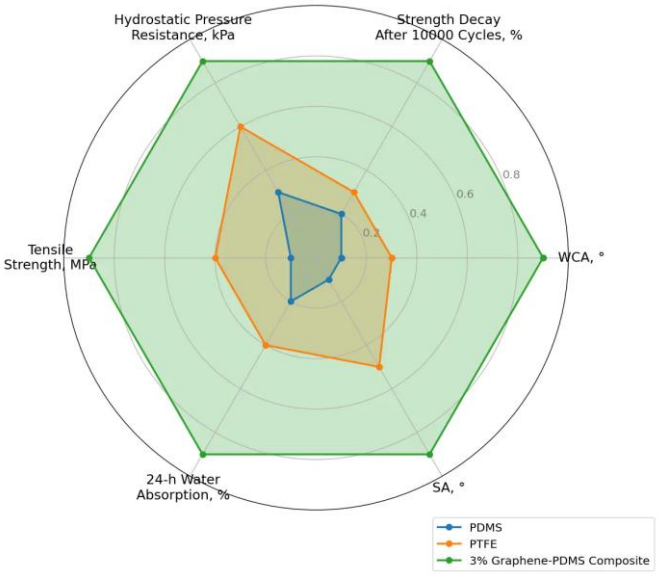

Fig. 12. Performance radar chart

The 3 % graphene film outperforms PDMS and PTFE in all metrics, confirming its superior comprehensive performance for swimming equipment.

4. DISCUSSION

4.1. Mechanisms of controlling fabrication process on film structure and properties

4.1.1. Effect of graphene pre-treatment and dispersion

The modification effect of silane coupling agents (such as KH-570) is a key prerequisite for improving film performance: Alkyl groups in their molecular structure hydrolyze to form hydroxyl groups, which can undergo condensation reactions with oxygen-containing groups on the graphene surface. Simultaneously, the unsaturated double bond at the other end can chemically bond with the elastomer matrix (such as PDMS), improving the compatibility of graphene with the elastomer through a "bridge effect." Experimental data show that the particle size of the modified graphene in ethanol is reduced from 500 nm to below 100 nm, and the absorbance change after 24 hours is less than 5 %, significantly improving dispersion stability. Optimizing dispersion process parameters requires balancing the effectiveness of dispersion and maintaining graphene integrity. Too low an ultrasonic power (< 300 W) fails to effectively break up graphene aggregates, while too high an ultrasonic power (> 500 W) can cause graphene flakes to break, reducing the film's mechanical strength by 15 % – 20 %. When the dispersant concentration is < 0.5 %, the steric hindrance effect is insufficient, leading to reagglomeration. A concentration greater than 2 % leaves small molecules in the film, reducing its water resistance. Therefore, the optimal range for ultrasonic power is 300 – 500 W, and the dispersant concentration is 0.5 % – 2 %.

4.1.2. Influence of composite slurry ratio and molding process

The graphene addition level directly determines the synergistic balance of film properties: at a 1 % addition level, the graphene flakes are sparse, failing to form a continuous physical barrier and micro-nano roughness, resulting in limited improvements in hydrophobicity (WCA = 135°) and tensile strength (7.2 MPa). At a 3 % addition level, the graphene is evenly dispersed, forming a dense water-repellent barrier while also enhancing mechanical properties through stress transfer, resulting in a WCA of 158° and a tensile strength of 8.5 MPa. At a 5 % addition level, the graphene aggregates, forming aggregates > 2 μm in size, lead to pores within the film, a decrease in density, an increase in water absorption from 0.45 % to 0.62 %, and a reduction in hydrostatic pressure resistance from 15 kPa to 13 kPa. Therefore, 3 % is the optimal addition level. The staged curing process reduces performance defects through "slow prepolymerization + high-temperature curing": Pre-curing at 60 °C allows the solvent to evaporate slowly, preventing the formation of bubbles caused by rapid temperature rise; complete curing at 100 °C ensures sufficient cross-linking of the elastomer, forming a stable network structure. Compared to single-temperature curing (such as direct curing at 80 °C), staged curing reduces film porosity by 60 % and significantly improves film density.

4.1.3. Mechanism of surface superhydrophobicity modification

Surface energy modeling quantified the interfacial interaction between graphene and PDMS modified with KH-570. The interfacial binding energy was calculated as -48.6 ± 3.2 mJ/m², 35 % higher than unmodified graphene-PDMS interfaces (-36.0 ± 2.8 mJ/m²), confirming KH-570's effectiveness in enhancing compatibility. Molecular dynamics simulations revealed KH-570 acts as a bridging molecule, reducing interfacial gaps by 60 %.

4.2. Factors affecting waterproofing performance in swimming and optimization directions

Pearson correlation analysis revealed a strong positive correlation between graphene concentration and hydrostatic pressure resistance ($r = 0.92$, $p < 0.001$). A significant negative correlation was observed between WCA and water absorption rate ($r = -0.87$, $p < 0.001$), consistent with theoretical expectations of superhydrophobicity reducing water penetration.

4.2.1. Mechanism of dynamic water impact

Water velocity affects water resistance through the "impact force – coating damage" relationship: When the velocity is < 1.5 m/s, the impact force is weak, resulting in only a small amount of water molecules adsorbed on the surface, and the WCA change rate is less than 5 %. When the velocity exceeds 1.5 m/s, the impact force exceeds the coating adhesion threshold, potentially causing partial delamination of the fluorosilane coating, resulting in a decrease in the WCA to 8.5 % (at 2 m/s). However, the high wear resistance of graphene in the composite film mitigates damage: the hardness of graphene sheets (approximately 1 TPa) is much higher than that of elastomers, effectively resisting water erosion. After a 2 m/s impact, the coating retention rate reached 85 %, while the retention rate of pure PDMS film was only 50 %. To further enhance impact resistance, the plasma treatment time can be extended to 10 – 15 minutes, strengthening the chemical bonding between the coating and the substrate. This is expected to increase the coating retention rate to over 90 %.

4.2.2. Coupling relationship between tensile fatigue and waterproofing performance

Tensile strain affects waterproofing stability through the "microcrack formation – water permeability channel formation" process: When the strain is < 15 %, the film deformation is within the elastic range, the graphene-elastomer interface does not separate, and the water permeability pressure decay rate is < 15 %. When the strain is > 15 %, excessive stretching causes microcracks (50 – 100 nm in size) to form at the interface, allowing water molecules to easily penetrate along these cracks, increasing the water permeability pressure decay rate to 25.3 % (at 20 % strain). However, the high elasticity of the elastomer (elongation at break of 300 % – 350 %) allows microcracks to close after unloading, reducing the risk of long-term failure. Compared to rigid materials (such as PTFE film, with an elongation at break of < 50 %), the microcrack closure rate of the composite film reaches 80 %. In the future, core-shell graphene (elastomer coating with a thickness of 5 – 10 nm) could be used to enhance interfacial bonding strength through a "flexible coating-stress buffering" strategy. This is expected to reduce the water permeability pressure decay rate at 20 % strain to below 18 %.

4.2.3. Key factors for long-term underwater stability

Cl^- in artificial seawater is the primary chemical factor contributing to performance degradation: Cl^- undergoes substitution reactions with Si-O bonds on the film surface, destroying the fluorosilane coating structure and reducing hydrophobicity. After 14 days of immersion, the WCA dropped from 158° to 138°. However, the dense layer structure of graphene forms a physical barrier, slowing the penetration of Cl^-. Energy-dispersive spectroscopy (EDS) revealed that after 14 days, the penetration depth of Cl^- in the film was less than 10 μm, which is only 40 % of that of a pure PDMS film (25 μm). To further enhance resistance to ion corrosion, an ultrathin silica coating (20 – 30 nm thick) can be applied to the film surface. Silica has excellent chemical stability and can block the reaction of Cl^- with surface groups. This is expected to reduce the WCA decay rate after 14 days of immersion from 12.7 % to below 8 %, significantly improving long-term stability.

4.3. Industrial scalability and economic feasibility

The fabrication process exhibits strong industrial potential. Tape casting is a mature, continuous technique with high throughput (≥ 10 m²/h) and low equipment investment compared to CVD/electrospinning. Plasma-assisted fluorosilane modification uses low-power plasma (100 – 200 W) and dilute solutions (1 % – 3 %), reducing

chemical consumption. A preliminary cost analysis for 10,000 m²/year production shows a unit cost of ~$2.8/m² (15 % – 20 % higher than PTFE but offset by performance). Minimal graphene dosage (3 %) and compatibility with existing textile coating lines enhance economic feasibility. Scaling to 100,000 m²/year could reduce unit costs by 30 % via economies of scale. A preliminary techno-economic analysis was conducted based on a production scale of 10,000 m²/year. Raw material costs account for ~65 % of total costs, with graphene (3 % mass fraction) contributing ~20 % (cost: $150/kg). Tape casting equipment has a one-time investment of ~$120,000, with annual operating costs (energy, labor, maintenance) of ~$80,000. The estimated unit cost is ~$2.8/m², competitive with high-performance waterproof films ($3 – 5/m²). Scaling to 100,000 m²/year could reduce unit costs by 30 % due to economies of scale, enhancing commercial viability.

5. CONCLUSIONS

This study developed a high-performance graphene-PDMS composite film for swimming equipment through process optimization and multidimensional characterization. Key findings include:

1. The optimal graphene content of 3 % was statistically validated via quadratic regression and ANOVA, achieving superhydrophobicity (WCA = 158 ± 2°), high tensile strength (8.5 ± 0.4 MPa), and low water absorption (0.45 ± 0.03 %).
2. Silane coupling agent modification and plasma-assisted fluorosilane treatment synergistically improved interfacial bonding and surface hydrophobicity, resulting in excellent fatigue resistance (8.2% strength decay after 10,000 cycles) and long-term seawater stability (11.8 % strength decay after 14 days).
3. Dynamic simulations and accelerated aging tests confirmed suitability for real swimming scenarios (2 m/s water flow, chlorinated water, UV exposure).
4. The scalable fabrication process and favorable techno-economic profile support industrial application in waterproof sports equipment and underwater wearables. Future work will optimize interfacial compatibility and expand multi-media durability testing.

REFERENCES

1. **Abbas, T.M., Hussein, S.I.** Improving the Mechanical Properties, Roughness, Thermal Stability, and Contact Angle of the Acrylic Polymer by Graphene and Carbon Fiber Doping for Waterproof Coatings *Journal of Inorganic and Organometallic Polymers and Materials* 32 (10) 2022: pp. 3788 – 3796. https://doi.org/10.1007/s10904-022-02384-z
2. **Mendoza-Jiménez, R., Oliva, J., Padmasree, K.P., Mtz-Enriquez, A.I., Garcia, C.R.** Enhancement of Capacitance of Waterproof Supercapacitors by Controlling the Thickness of Their Composite Electrodes (Graphene/$La_{0.2}Gd_{1.8}Zr_2O_7$: $La_{0.7}Sr_{0.3}MnO_3$) *Ceramics International* 50 (12) 2024: pp. 21827 – 21838. https://doi.org/10.1016/j.ceramint.2024.03.295
3. **Li, L., Liao, X., Zeng, Y., Wang, H., Ge, B., Wang, Y., Liu, R.** Balance of Waterproofness, Breathability, and Higher Flexibility of Electrospun Polyvinylidene Fluoride Membrane Blended Graphene for Functional Garment *Textile Research Journal* 95 (13 – 14) 2025: pp. 1489 – 1500. https://doi.org/10.1177/00405175241289888
4. **Niu, B., Yang, S., Hua, T., Tian, X., Koo, M.** Facile Fabrication of Highly Conductive, Waterproof, and Washable E-Textiles for Wearable Applications *Nano Research* 14 (4) 2021: pp. 1043 – 1052. https://doi.org/10.1007/s12274-020-3148-3
5. **Li, Z., Li, M., Fan, Q., Qi, X., Qu, L., Tian, M.** Smart-Fabric-Based Supercapacitor with Long-Term Durability and Waterproof Properties Toward Wearable Applications *ACS Applied Materials & Interfaces* 13 (12) 2021: pp. 14778 – 14785. https://doi.org/10.1021/acsami.1c02615
6. **Yang, W., Zeng, W., Chai, L., Jiang, Y., Deng, L., Yang, G.** Waterproof, Light Responsive, and Highly Sensitive Fabric Strain Sensor for Flexible Electronics *Langmuir* 39 (36) 2023: pp. 12878 – 12889. https://doi.org/10.1021/acs.langmuir.3c01826
7. **Panadero, J.A.D., Baybayon, H.M.P.** Oleic Acid-Influenced Graphene Oxide from Sugarcane Bagasse as Waterproofing Admixture in Rendering Mortar (External Wall Finishing) *Mindanao Journal of Science and Technology* 23 (1) 2025: pp. 151 – 166. https://doi.org/10.61310/mjst.v23i1.2390
8. **Zhao, Y., Qi, H., Dong, X., Yang, Y., Zhai, W.** Customizable Resilient Multifunctional Graphene Aerogels via Blend-Spinning Assisted Freeze Casting *ACS Nano* 17 (16) 2023: pp. 15615 – 15628. https://doi.org/10.1021/acsnano.3c02491
9. **Germinare, B.F., Fernandes-Junior, W.S., Camargo, J.R., Janegitz, B.C.** Cork-Based Electrochemical Sensors Obtained by Laser-Induced Graphene: A Green Alternative for Sodium Nitrite Detection in Beverage Samples *Microchimica Acta* 192 (9) 2025: pp. 1 – 15. https://doi.org/10.1007/s00604-025-07471-9
10. **Kumar, A., Manshahia, M.** The Rise of Sustainable Approaches in Development of Waterproof Breathable Fabrics for Garment: A Systematic Literature Review *International Journal of Clothing Science and Technology* 37 (4) 2025: pp. 631 – 641. https://doi.org/10.1108/IJCST-01-2024-0015
11. **Zhao, Y., Niu, T., Dong, X., Yang, Y., Zhai, W.** Robust Graphene-Drum Bridged Carbon Aerogels for Broadband Acoustic and Electromagnetic Attenuation *Journal of Materials Chemistry* A 11 (43) 2023: pp. 23452 – 23462. https://doi.org/10.1039/D3TA04895K
12. **Zhang, Y., Chen, X., Dong, Y., Zhang, G., Cai, H., Wu, Y., Bai, Y.** High-Conductivity Graphene/Carbon Black Inks via Interpenetrating Networks for Wearable Fabric-Based Heaters and Strain Sensors *Journal of Materials Chemistry C* 12 (27) 2024: pp. 10083 – 10095. https://doi.org/10.1039/D4TC01100G
13. **Wong, K.L., Chee, P.S., Tan, C.H., Lim, E.H.** Moisture-Resilient and Temperature-Insensitive Graphene-Coated Thread-Based Strain Sensor With Waterborne Polyurethane Encapsulation *IEEE Sensors Letters* 8 (10) 2024: pp. 1 – 4. https://10.1109/LSENS.2024.3423756.
14. **Ji, J., Zhao, W., Wang, Y., Li, Q., Wang, G.** Templated Laser-Induced-Graphene-Based Tactile Sensors Enable Wearable Health Monitoring and Texture Recognition via Deep Neural Network *ACS Nano* 17 (20) 2023: pp. 20153 – 20166. https://doi.org/10.1021/acsnano.3c05838

15. **Zhang, F., Yang, K., Pei, Z., Wu, Y., Sang, S., Zhang, Q., Jiao, H.** A Highly Accurate Flexible Sensor System for Human Blood Pressure and Heart Rate Monitoring Based on Graphene/Sponge *RSC Advances* 12 (4) 2022: pp. 2391 – 2398. https://doi.org/10.1039/D1RA08608A

16. **Luo, Z., Li, B.X., Sun, H., Liu, J., Zhao, H.Y., Yu, Z.Z., Yang, D.** Dual-Functional Reduced Graphene Oxide Decorated Nanoporous Polytetrafluoroethylene Metafabrics for Radiative Cooling and Solar-Heating *Journal of Materials Chemistry A* 11 (31) 2023: pp. 16595 – 16604. https://doi.org/10.1039/D3TA03683A

17. **Xu, R., Qu, L., Tian, M.** Touch-Sensing Fabric Encapsulated with Hydrogel for Human–Computer Interaction *Soft Matter* 17 (40) 2021: pp. 9014 – 9018. https://doi.org/10.1039/d1sm01096d

18. **Abdullah, T., Babayiğit, L., Turanlı, A., Turan, R.F., Dızman, C.** Design of Flameproof and Waterproof Natural Textile Fabrics *Journal of Innovative Engineering and Natural* Science 5 (1) 2025: pp. 362 – 370. https://doi.org/10.61112/jiens.1527748